

Impact of Infill Density and Glass Fiber Reinforcement on the Compressive and Bending Strength of Acrylonitrile Butadiene 3D-Printed Corrugated Sandwich Panels

Ali Sadooghi, Mohammad Reza Ebrahimian,* Seyed Jalal Hashemi, Rasool Sayar, Kaveh Rahmani, and Mahdi Bodaghi*

Sandwich panel structures are widely utilized across various industries due to their exceptional strength-to-weight ratios, particularly when employing a corrugated core. In this study, the innovative use of additive manufacturing and fused deposition modeling to produce corrugated core sandwich panels with enhanced mechanical properties are investigated. Acrylonitrile butadiene styrene filaments reinforced with varying percentages of glass fibers (0, 5, 10, and 15%) are utilized, and three distinct infill density patterns are examined. The panels are subjected to three-point bending and compressive tests, revealing that a 10% glass fiber reinforcement yields the highest bending (1973.62 N) and compressive strengths (9581.56 N). Beyond this reinforcement level, strength decreases due to fiber agglomeration. Microstructural analysis using scanning electron microscope confirms optimal dispersion and bonding of glass fibers at 10%, which improves mechanical performance. Thermal analysis identified the appropriate printing temperatures, ensuring high-quality layer adhesion. The novel approach of varying infill densities and fiber content contributes to optimizing 3D printing parameters, advancing the production of lightweight, high-strength structures for applications in automotive, aerospace, and construction industries. In this study, significant insights into the relationship between material composition, manufacturing parameters, and mechanical properties of 3D-printed sandwich panels are provided.

structures involve multiple complex stages, making production costly and necessitating the use of intricate and occasionally challenging equipment.^[1] With the advancements in various manufacturing methods, new materials, and filaments, researchers' attention to 3D printers has increased more than ever. The continuous improvement of the process and the production of parts with higher strength for samples produced by this method have always been of interest to industry professionals. The 3D printers do not use a similar technology for product manufacturing, and the major difference in these technologies lies in the method of layering to create the final product. One of these methods is fused deposition modeling (FDM), where materials capable of melting are used to produce layers and samples.^[2] The 3D printers with FDM technology use thermoplastics in filament form as their consumables, with one of the most common being acrylonitrile butadiene styrene (ABS) filaments, known for their high melting temperature, flexibility, and suitable strength.^[3]

To improve the quality, increase strength, and mechanical properties of filaments and produced samples, reinforcements such as particles and fibers are sometimes added to the filament, with one of the most common being glass fibers. Sedlak et al.^[4] used a 3D printer to produce samples with different filaments for hardness, tensile, and bending tests. The results of the tests and extraction of the mechanical properties of the

1. Introduction

Sandwich panel structures, due to their superior flexural stiffness-to-weight ratio, are utilized in various industries such as automotive, sustainable energy, aerospace, and construction. Traditional manufacturing and assembly methods for lightweight sandwich

A. Sadooghi, S. J. Hashemi
Department of Mechanical Engineering
National University of Skills (NUS)
Tehran 36471-13736, Iran

 The ORCID identification number(s) for the author(s) of this article can be found under <https://doi.org/10.1002/adem.202401842>.

© 2024 The Author(s). Advanced Engineering Materials published by Wiley-VCH GmbH. This is an open access article under the terms of the Creative Commons Attribution License, which permits use, distribution and reproduction in any medium, provided the original work is properly cited.

DOI: 10.1002/adem.202401842

M. R. Ebrahimian, R. Sayar
Department of Mechanical Engineering
Kar Higher Education Institute
Qazvin 34318-49689, Iran
E-mail: m.ebrahimian@kar.ac.ir

K. Rahmani, M. Bodaghi
Department of Engineering
School of Science and Technology
Nottingham Trent University
Nottingham NG11 8NS, UK
E-mail: mahdi.bodaghi@ntu.ac.uk

produced samples showed that the use of polylactic acid (PLA) filaments is optimal in terms of cost. Wu et al.^[5] used polyamide and polymer materials for medical applications to produce sandwich panels with a 3D printer and calculated their mechanical properties through mechanical tests. Zaharia et al.^[1] produced samples with polymer filaments using additive manufacturing methods, which were sandwich panel structures, and conducted a three-point bending test on them. They experimentally determined their strength and then numerically simulated them. Gaoyuan et al.^[6] designed a truss structure and printed a sample using a pyramid filament and a 3D printer, obtaining the mechanical properties of the designed structure through compressive and energy absorption tests. Yap et al.^[7] produced samples with ABS filaments reinforced with polycarbonate using FDM method and examined their tensile and bending properties. The samples were printed at different speeds, percentages of infill density, and nozzle diameters and were tested. Based on the obtained results, the ideal process parameters were determined to be a speed of 60 mm s^{-1} , infill density of 15%, and nozzle diameter of 0.8 mm, resulting in a 38.46% improvement in tensile strength, 23.40% in modulus of elasticity, and 23.90% in bending strength. Coppola et al.^[8] produced PLA filaments with a diameter of 1.75 mm that were reinforced with nanocomposite clay particles and printed samples at different nozzle temperatures. The samples were subjected to thermal analysis and tensile tests, and the results showed that the presence of clay nanoparticles improved thermal stability and increased the modulus of elasticity. Also, increasing the printing temperature led to the production of samples with higher strength. Ferreira et al.^[9] obtained the mechanical properties of printed samples with PLA filaments reinforced with carbon fibers. The variable parameters of the produced samples were layering and different printing orientations, and subsequently, mechanical properties such as strength, shear modulus, and Poisson's ratio of the samples were analyzed. Ye et al.^[6] designed pyramid lattice truss structures and produced them using additive manufacturing method, examining the mechanical properties and energy absorption of the samples. The samples were printed horizontally and vertically, both patterns showing similar mechanical properties, with the vertically printed samples demonstrating better deformability. Wannarong et al.^[10] reviewed articles on sandwich panel samples produced using additive manufacturing with PLA and ABS filaments. The research showed that ABS printed samples had higher bending strength and elongation compared to PLA, and the bending and fatigue properties of sandwich panel structures depended on density, design, core structure, thickness, and infill density. Yousefi et al.^[11] produced novel 3D printing meta structures by thermoplastic polyurethane filament and then single and cyclic loading-unloading tests with the aim of absorption/dissipation applications were done on the sample. The feasibility and mechanical performance of different meta-structures are assessed experimentally and numerically. Computational finite-element models for the meta-structures are developed and verified by the experiments. Hamzehei et al.^[12] designed a novel bioinspired metamaterial and manufactured additively and the mechanical properties were investigated experimentally and numerically in micro- and macroscales. Also the obtained results were compared to some traditional lattice structures. Rahmatabadi et al.^[13]

produced additively some shape memory polymers parts and their behavior investigated by assessing fixity, shape recovery, stress recovery, and stress relaxation under bending and compression loading modes, also the transition. Furthermore, several researchers have conducted studies and published articles on the effect of infill density on the mechanical properties of FDM-printed parts. Yadav et al.^[14] printed PLA parts using the FDM method with varying infill densities from 20% to 80%. Compressive tests were conducted on the produced samples, and the results showed that for all samples and patterns, the compressive strength increased with increasing infill density of the core of the parts. In a similar study, Mishra et al.^[15] produced PLA parts using the FDM method and investigated the effects of different parameters such as printing pattern and infill density on their strength and absorbed energy. The results showed that the best results were obtained for samples with an infill density of 80%. Agrawal et al.^[16] produced ABS samples using the FDM method, and the samples were produced with different parameters of printing pattern, infill density, and layer thickness. Their mechanical properties were investigated. The results showed that the best mechanical properties were obtained for samples with a layer thickness of less than $100 \mu\text{m}$ and an infill density of 80%. Based on a review of previous research, few studies have been conducted on the effect of varying infill densities on mechanical properties. Tanveer et al.^[17] produced PLA parts according to the standard tensile and impact test using FDM method. Samples were produced with both constant and variable infill densities, where the infill density was considered in the cross section of the sample. The results showed that samples with variable infill density had higher tensile strength. Wegner et al.^[18] used optimization algorithms to design a printing pattern and variable infill density to produce parts using the FDM method. The aim of this optimization was to achieve the highest flexural strength. In a similar study, Cheng et al.^[19] optimized the infill density of a cantilever beam to obtain a higher natural frequency for the structure.

This study investigates the novel use of additive manufacturing to enhance the mechanical properties of corrugated core sandwich panels. ABS filaments reinforced with varying percentages of glass fibers (0, 5, 10, and 15%) were utilized to fabricate samples with three distinct infill density patterns: a constant 50% density, a gradient from 15% to 60%, and a variable density from 25% to 75% at critical points. The objective was to analyze how these parameters affect the bending and compressive strengths of the panels. No prior research has comprehensively examined the combined effects of these variables on corrugated core sandwich structures. Microstructural analysis using scanning electron microscope (SEM) confirmed that 10% glass fiber reinforcement optimally disperses and bonds within the ABS matrix, leading to improved mechanical performance. Experimental results showed significant enhancements in bending and compressive strengths, particularly with the 10% reinforcement and optimized infill patterns. This study provides valuable insights into the optimization of 3D printing parameters for developing high-strength, lightweight structures, contributing significantly to the fields of automotive, aerospace, and construction.

2. Experimental Section

2.1. Filament Production

ABS filaments reinforced with glass fibers were extruded to improve the quality and strength of ABS filaments. To produce filaments that do not deform, ABS granules were dried at 800 °C, then short glass fibers were milled using a planetary mill to reach a fiber size of $\approx 500 \mu\text{m}$ and an L/D ratio of 300 m. Subsequently, using a single-screw extruder at a rotational speed of 300 rpm, ABS granules with different percentages of glass fibers (0, 5, 10, and 15%) were uniformly mixed, melted, extruded at a pressure of 6 MPa, and passed through cold water to prevent distortion and heterogeneity in the produced filaments. Tensile tests were conducted on the produced filaments to determine their tensile properties. Additionally, thermal analysis test was performed on the produced filaments to assess their thermal properties and select the appropriate printing temperature. Adjusting the nozzle temperature according to the filament for printing resulted in better adhesion between layers and production of samples with improved mechanical strength.^[20] In **Figure 1**, milled glass fibers, rolls of ABS filaments reinforced with 15% glass fibers with a diameter of 1.75 mm, and the process of conducting tensile tests on the produced filaments could be observed.

2.2. Samples' Design and Production

Sample designs were created using Solid Work 2014 software, with dimensions of 121×33 mm and edge thickness ranging from 4 to 5 mm as shown in **Figure 2**.

A series of samples were printed using same infill density setup in the software equal to 50%; these samples were labeled with the pattern name Pattern 1 (P1). When a sample was subjected to bending loads, the bending stress created had a direct

relationship with the bending moment which changed the bending stress. Thus, another pattern for infill density was selected where the infill percentage increased from 15% at the center of the sample to 60% at the farthest points from the center in five stages, named Pattern 2 (P2). Another pattern was chosen based on the stress distribution that this sandwich panel structure with a corrugated core withstood under bending loads. Accordingly, samples were divided into different regions and printed with varying percentages of infill density ranging from 75% at force application points to 25% at the edges, named Pattern 3 (P3). Schematic images of infill density patterns for samples can be seen in **Figure 3**. All samples were produced by FDM method and using filaments reinforced with different percentages of glass fibers (0, 5, 10, and 15%) and printed with a brass nozzle printer with a diameter of 0.4 mm, nozzle temperature of 230 °C, bed temperature of 90 °C, speed of 60 mm s^{-1} , layer height of 0.15 mm, and triangle infill pattern. The printed samples were labeled according to the pattern and filament type used for printing in **Table 1**.

2.3. Bending Test

To perform the three-point bending test, the sample was placed on two supporting bases, and a movable arm applied a force at a specific point on the sample, the midpoint between the two supporting bases. The three-point bending test was conducted to find the displacement and bending force of the sandwich panel structure with a corrugated core on a Zwick Rowell universal testing machine model Z100 with a preload of 2 N, a force application speed of 5 mm min^{-1} , and a support span of 7 mm according to the test condition of ASTM D790. A schematic image of the force application and the bending test conducted on the printed sample can be seen in **Figure 4**.

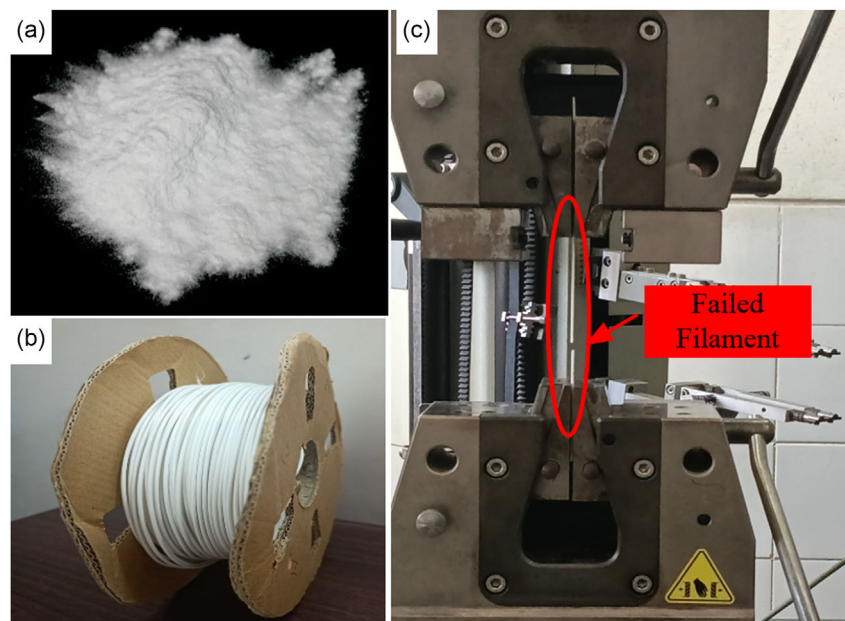


Figure 1. a) The milled glass fiber, b) the produced ABS-15% glass fiber filament, and c) the end of tensile test of filament.

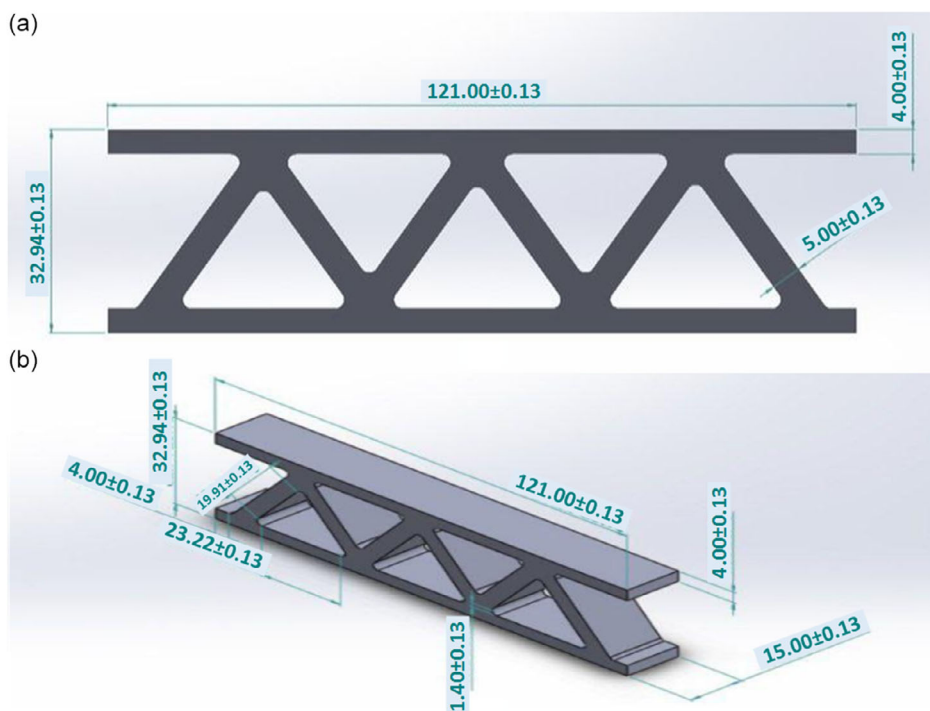


Figure 2. The dimension of designed sample from a) front view and b) 3D view.

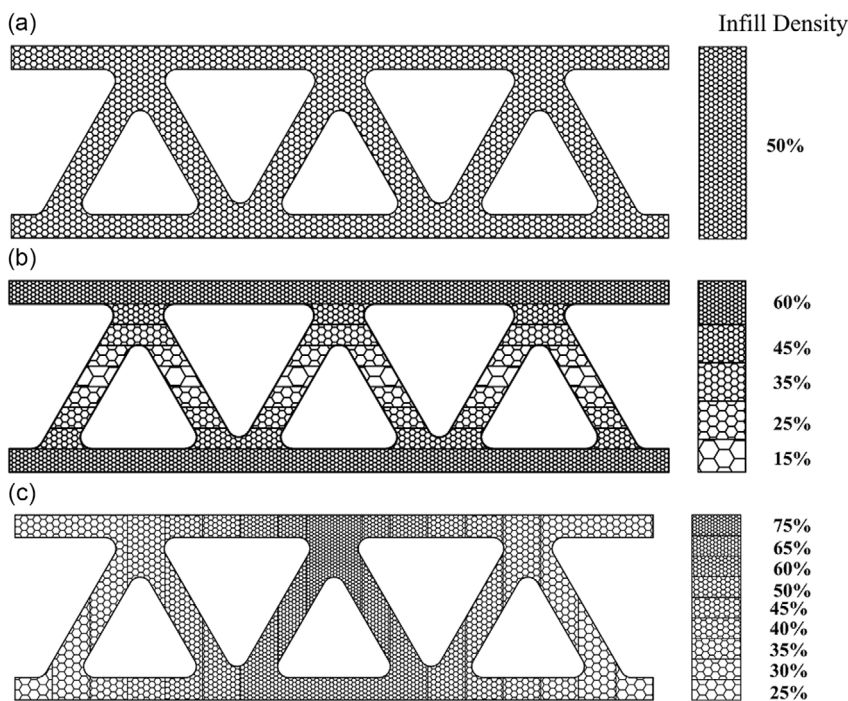


Figure 3. The schematic of infill density distribution of sample: a) P1, b) P2, and c) P3.

2.4. Compressive Test

For the compressive test, the samples were placed on the base of the machine in a way that the entire bottom layer of the

sample was on the support, and a movable arm applied a force extensively on the top layer of the sample. The compressive test was conducted to find the displacement and compressive force of the printed samples with a preload of 2 N and a force

Table 1. The produced samples specification.

Samples' name	Filament				
	ABS-0% glass fiber	ABS-5% glass fiber	ABS-10% glass fiber	ABS-15% glass fiber	
Pattern	P1	P10	P15	P110	P115
	P2	P20	P25	P210	P215
	P3	P30	P35	P310	P315

application speed of 5 mm min^{-1} . Images related to the compressive test along with its schematic image can be seen in **Figure 5**.

3. Results and Discussion

3.1. Filament Analysis and Sample Production

To ensure the quality of the produced filaments and to examine the dispersion and proper bonding between glass fibers and the ABS base material, filaments reinforced with 15% glass fiber were cut and placed under SEM imaging. The images related to this are magnified differently in **Figure 6**, where the presence of glass fibers in the base material is evident, and their proper bonding with the base material is marked. The indication of this is the adhesion of ABS base material in particle form along the surface of the glass fibers.^[21] Based on the scale of **Figure 6**, it can be observed that the diameter of the glass fibers is $\approx 5 \mu\text{m}$, and the ABS base material and glass fibers are homogeneously

mixed. No fiber agglomeration is observed, and due to the varied distribution of fibers, isotropic behavior of the filament can be expected. Additionally, to achieve tensile properties, tensile tests were performed on all produced filaments, and the results and graphs are presented in **Table 2** and **Figure 7**. Based on the results obtained, the highest failure force for ABS-10% glass fiber filament was found to be 103.39 N, which is 13% higher than the failure force of ABS-0% glass fiber filament. This increase is due to the presence of glass fibers in the base material, which allows for higher force tolerance, delayed fracture, and consequently greater elongation at the time of fracture. Increasing glass fibers up to 15% in the base material leads to brittleness, reduced deformability, and decreased breaking force. The elastic behavior of all four types of filaments in the tensile test is almost identical, and their Young's modulus is similar. Based on the obtained graphs, it can be concluded that the necking phenomenon did not occur in the filament reinforced with 15% glass fibers, unlike the other three filaments. The most nonuniform deformation after necking was observed for the filament reinforced with 10% glass fibers, which delayed the fracture and increased the strain.

Since the nozzle temperature is one of the most important parameters for printing samples and the quality of the final sample directly depends on the printing temperature of the layers, to ensure the selection of the appropriate nozzle temperature, a thermal analysis test was performed on the produced filaments up to a maximum temperature of $280 \text{ }^\circ\text{C}$ with a temperature increase rate of $5 \text{ }^\circ\text{C min}^{-1}$. The results of this test are plotted in **Figure 8**. The obtained graphs showed that an increase in glass fibers in the filaments leads to an increase in their glass transition temperature, which is due to the presence of fibers in the

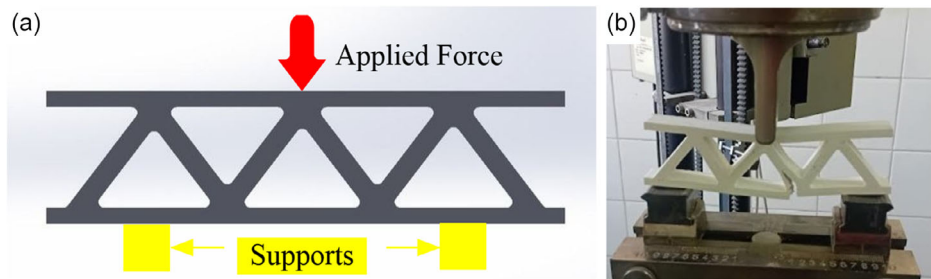


Figure 4. a) The schematic of bending test and b) the bending test.

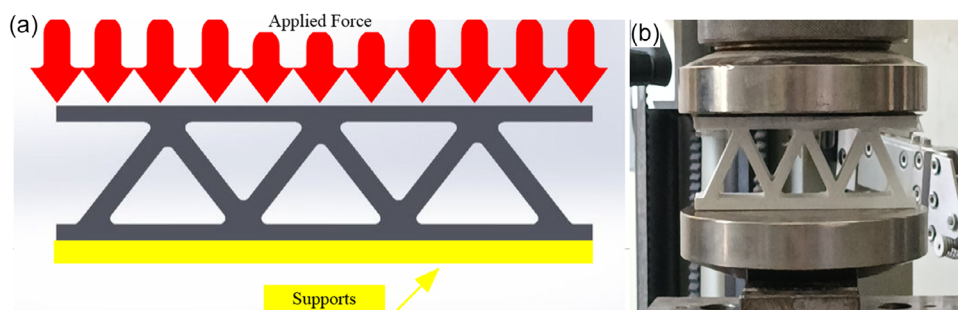


Figure 5. a) The schematic of compressive test and b) the compressive test.

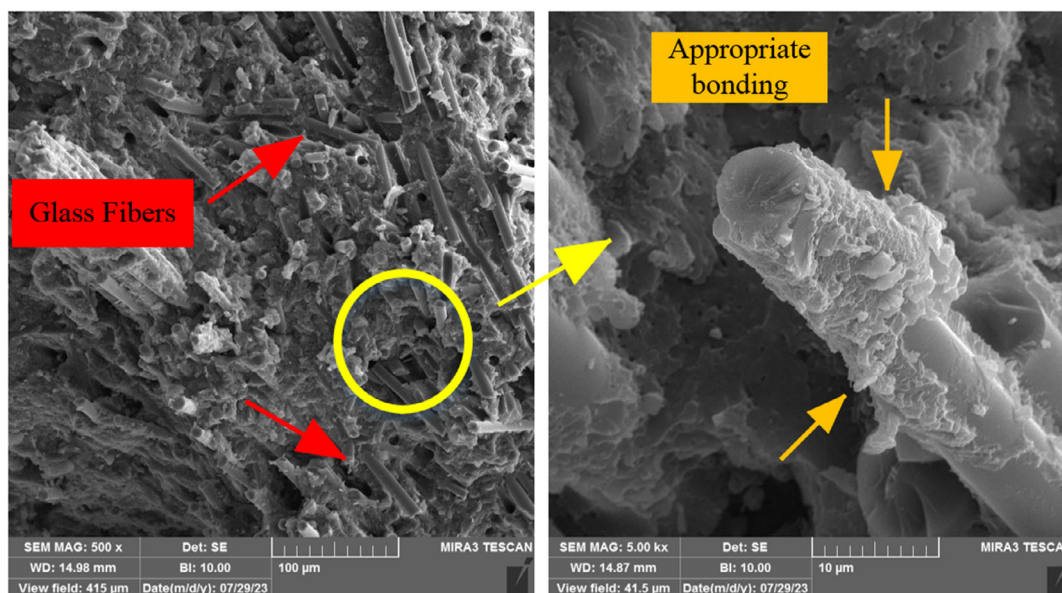


Figure 6. The SEM image of produced ABS-15% glass fiber filament.

Table 2. The tensile result of produced filaments.

Sample	Failure force [N]	Elongation [mm]
ABS-0% glass fiber	91.32	7.96
ABS-5% glass fiber	103.39	9.23
ABS-10% glass fiber	115.27	11.14
ABS-15% glass fiber	89.19	6.58

ABS base material and the reduced fluidity of the filament, affecting the movement of the ABS polymer.^[22] Additionally, since glass fibers are not thermal conductors, the thermal transfer of reinforced filaments decreases. As the percentage of glass fibers in the ABS base material increases, with an increase in temperature, the material transitions from a glassy state to a

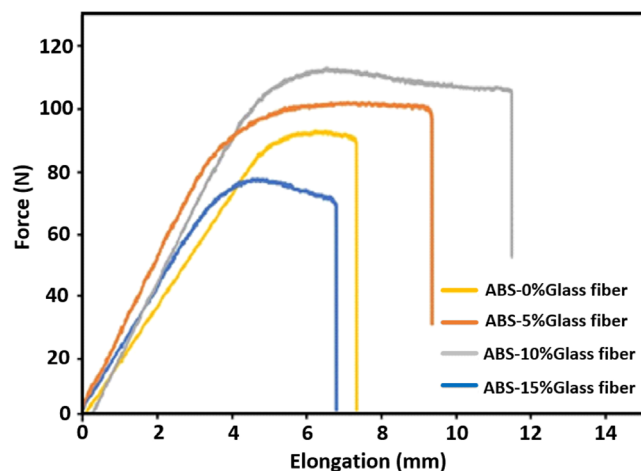


Figure 7. The force–elongation diagram of produced filaments.

plastic state. The glass transition temperature for ABS-0% glass fiber filament is ≈ 100 °C, while for ABS-15% glass fiber filament, it is determined to be 120 °C. Therefore, based on the differential scanning calorimeter (DSC) graph, a nozzle temperature of 230 °C was chosen for printing the samples, which does not create any disruption in sample production.

The designed samples, following the three mentioned patterns and with four different filament types, were printed. Images of the produced sample with ABS-0% glass fiber filament can be seen in Figure 9a. Since the samples were printed with three outer layers at 100% infill density, to ensure the accuracy of distribution and percentages of printed patterns, a sample was cut from the middle, and images related to it can be seen in Figure 9b.

3.2. The Result of Bending Test

All printed samples were subjected to bending tests, and the results are presented in graphs in Figure 10 and 11. The failure bending force for sample P10 was found to be 1669.21 N, which

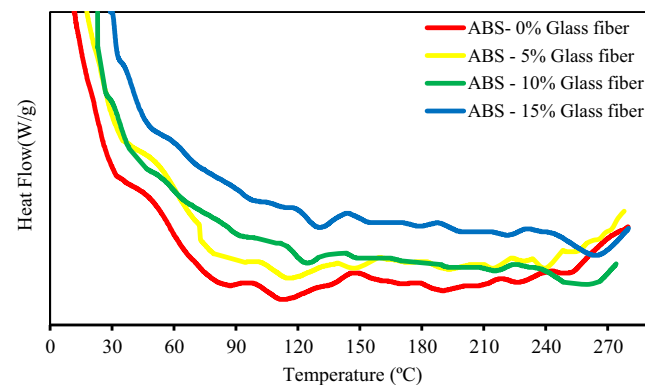


Figure 8. The DSC graph of produced filaments.

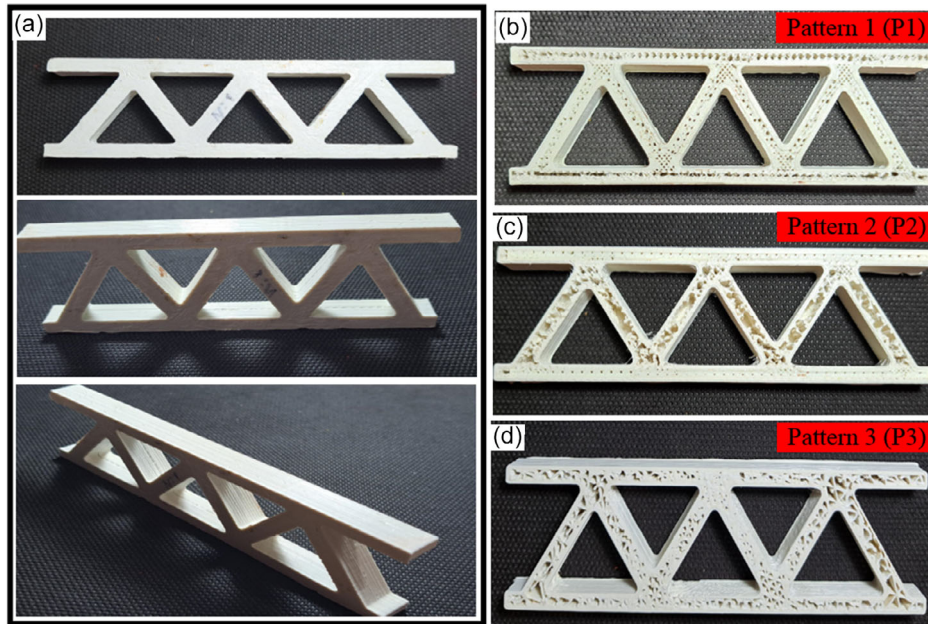


Figure 9. The produced sample with a) ABS-0% glass fiber filament, b) the pattern 1, c) the pattern 2, and d) the pattern.

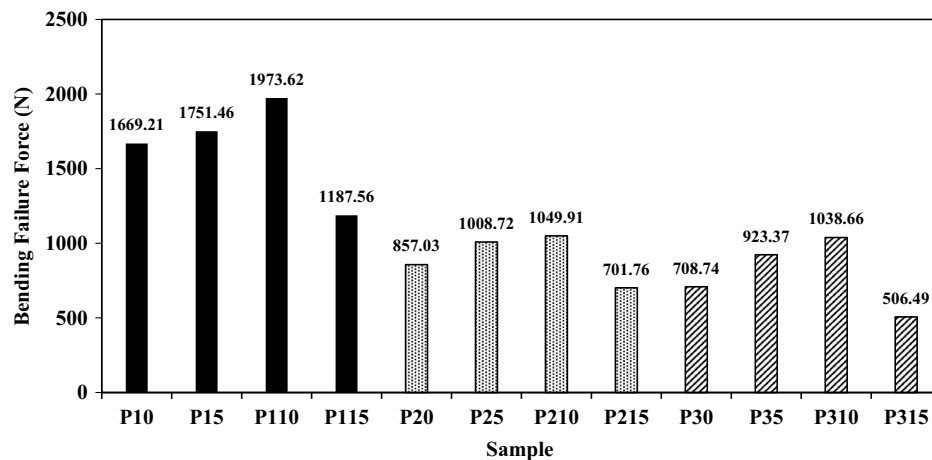


Figure 10. The obtained bending failure force of all produced samples.

increased with an increase in glass fibers in the filament base material for samples P15 and P110 to 1751.46 and 1973.62 N, respectively. Conversely, with an increase in the percentage of glass fibers from 10% to 15%, the failure bending force showed a decreasing trend, with a failure bending force of 1187.56 N obtained. A similar trend was also observed in displacement rates, with the highest displacement rate for sample P110 at 4.05 mm and the lowest displacement rate for sample P115 at 2.84 mm. The displacement rates for samples P10 and P15 were found to be 3.08 and 3.91 mm, respectively. The highest failure bending force and displacement among samples with pattern P2 were obtained for sample P210 at 1049.91 N and 3.57 mm, respectively, while the lowest failure bending force and displacement for sample P215 were found to be 701.76 N

and 2.69 mm, respectively. The lowest failure bending force for samples produced with pattern P3 was obtained for sample P315 at 506.49 N, while the highest failure bending force was obtained for sample P310 at 1038.66 N. In sample P35, with a decrease of 5% glass fibers in the ABS base material compared to sample P310, the failure bending force was determined to be 923.37 N. The displacement rate and failure bending force for sample P30 were found to be 2.77 mm and 708.74 N, respectively.

Generally, with an increase in the percentage of glass fibers up to 10% in the ABS base material, the failure bending force has increased. The reason for this phenomenon is the presence of glass fibers in the base material, which have proper dispersion and bonding with the base material. This allows the force to be

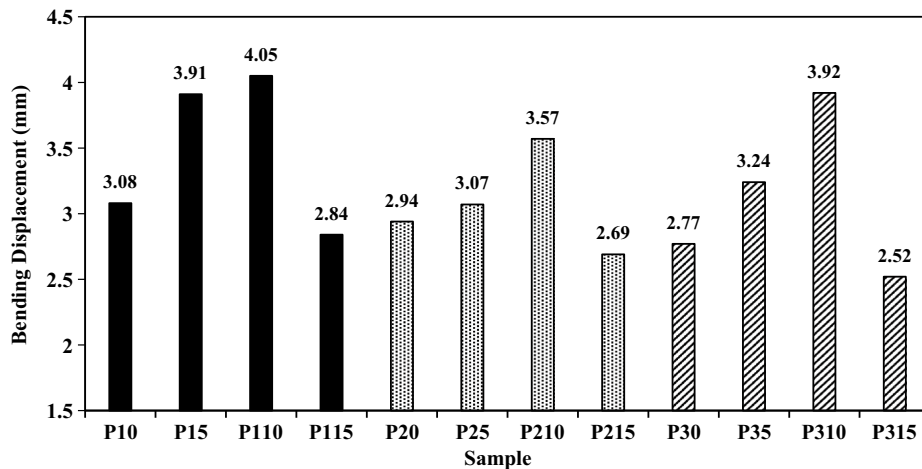


Figure 11. The obtained bending displacement of all produced samples.

borne by the glass fibers, leading to delayed fracture and increased breaking force. Another reason is the indication of a desirable printing process where suitable process parameters help achieve proper adhesion between layers. If the nozzle temperature or bed temperature is not selected appropriately, low-quality samples with poor adhesion between layers will be produced. The highest bending force in pattern P1 samples was obtained for sample P110 at 1973.62 N, which is 18% higher than the bending force of sample P10. In pattern P2, the highest bending force was obtained for sample P210 at 1049.91 N, which is 22% higher than the bending force of sample P20 at 857.03 N. However, the highest percentage increase in force was observed in samples produced with pattern P3, where the failure bending force for P30 increased by 46% from 708.74 to 1038.66 N. In contrast, with an increase in the percentage of glass fibers from 10% to 15%, a significant decreasing trend in the failure bending force of printed samples in all patterns was observed. The lowest failure bending force among all samples was obtained for sample P315 at 506.49 N, and the failure bending force for sample P215 was 701.76 N. The decreasing trend in the obtained forces can be attributed to the high percentage of glass fibers that agglomerate and cluster in the base material, leading to stress concentration in the sample. Additionally, a high percentage of glass fibers and their adhesion in the produced 1.75 mm filament can reduce print quality and ultimately decrease the strength of printed samples. The highest bending forces obtained for printed samples, regardless of the filament type used, were samples printed based on pattern P1, where all connections and areas were printed with a 50% infill density, improving the quality and integrity of the sample. With proper infill and sufficient layer adhesion, when applying force and transferring it in another direction, the force follows a longer path, leading to an increase in bending force at failure of the sample. Relatively, samples printed with pattern P2 tolerated slightly more bending force compared to samples printed with pattern P3, indicating that an increase in infill percentage from the center of the sample toward the edges leads to an increase in bending force at failure. A 60% infill density on the top and bottom surfaces of the sample, which bears the highest compressive and tensile forces,

helps improve this behavior. Pattern P3, due to slightly weaker infill percentages at connection points around 30–40%, leads to quicker failure in the sample. Comparing the displacement rates of all produced samples showed that an increase in the percentage of glass fibers up to 10% resulted in an increase in strain rate, and then with the addition of glass fibers reaching 15%, due to their agglomeration and clustering in the base material, premature failure occurred with a lower strain rate.

To better evaluate and validate the results, images of the failure of samples are provided in **Figure 12**, which are consistent with the results obtained. Due to variations in cross-sectional area and fiber orientation, a consistent cross-sectional area perpendicular to the applied load is absent, making accurate stress calculations extremely difficult. This, coupled with the complex and heterogeneous layered geometry of FDM-printed parts, renders stress–strain analysis challenging. Given these limitations, the samples' behavior was assessed based on failure load and elongation. The largest crack resulting from the failure of printed layers is observed in samples produced with filament reinforced with 15% glass fibers, indicating a completely brittle failure and severe delamination due to low adhesion between the layers. In contrast, a hairline and ductile failure is observed in samples printed with 10% glass fibers, indicating proper bonding between the layers and high resistance of the samples due to the presence and proper bonding between the glass fibers and the base material. In samples printed with filaments reinforced with 5% glass fibers, a relatively more ductile failure compared to samples printed with unreinforced filaments is observed. The failure of samples under bending force occurred at the joints of the samples, which is attributed to changes in cross-sectional area and stress concentration in the sample.

To investigate the behavior of samples under bending force, a force–displacement curve is provided in **Figure 13**. The trend of force–displacement curves for all samples, regardless of filament type and infill pattern, is similar, where with an increase in force, displacement in the samples continues until the moment of sample failure. A slight oscillation in the path of increasing force indicates the failure of printed layers progressing layer by layer and leading to final sample failure.



Figure 12. The images of fractured samples after bending test.

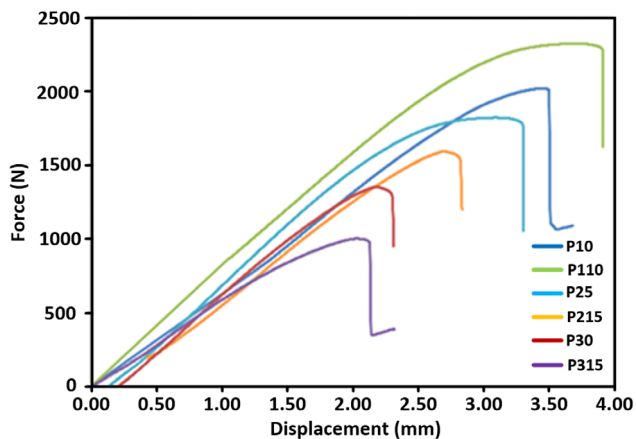


Figure 13. The force–displacement of samples after bending test.

3.3. The Result of Compressive Test

Compressive test was performed on the produced samples, and the results of failure compressive force and displacement of samples can be observed in **Figure 14** and **15**, respectively. In samples printed with pattern P1, where all areas had a 50% infill density, the highest and lowest compressive forces for samples P110 and P115 were obtained as 9581.56 and 4085.59 N, respectively, showing a 134% decrease with an increase in glass fiber percentage due to fiber clustering in the base material. The compressive force in sample P10 increased by 93% from 4714.61 to 9143.61 N with a 5% increase in glass fibers in the base material. A similar trend was also observed in displacement after compressive test in samples with pattern P1, where the highest and lowest displacement for samples P110 and P115 were 5.31 and 3.32 mm, respectively.

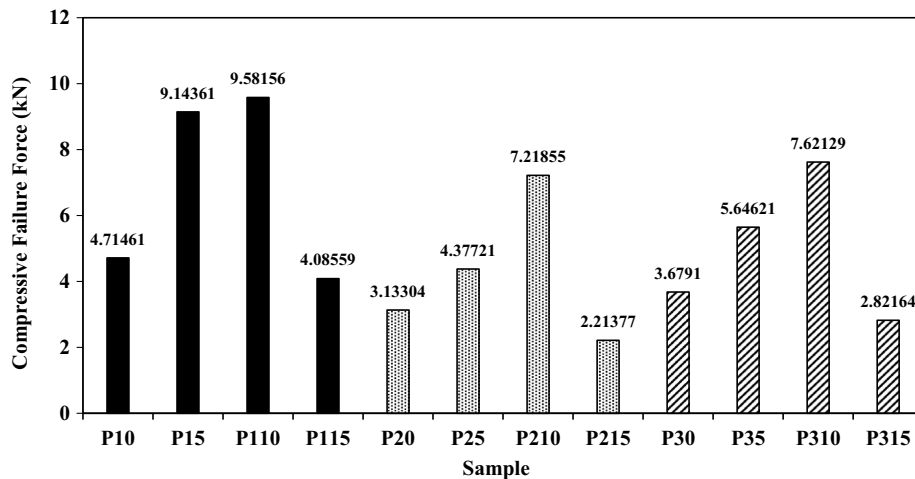


Figure 14. The obtained compressive failure force of all produced samples.

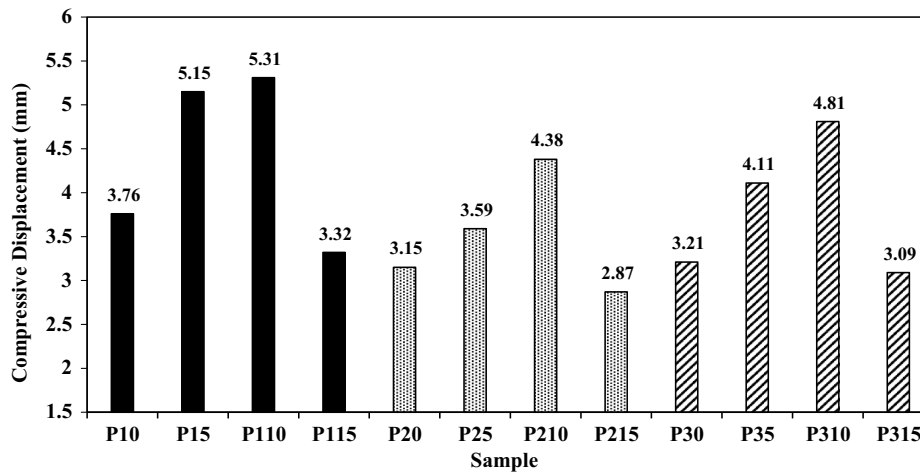


Figure 15. The obtained compressive displacement of all produced samples.

The compressive force in sample P20 was 3133.04 N, which increased to 7218.55 N with a 10% increase in glass fibers in the base material for sample P110. The lowest compressive force among samples printed with pattern P2 was obtained for sample P215 at 2213.77 N, with the lowest displacement for this sample being 2.87 mm. Among samples printed with pattern P3, the compressive force obtained for sample P30 was 3679.1 N, which increased by 53% to 5646.21 N in sample P35 with an additional 5% glass fibers added to the base material. Among pattern P3 samples, the highest compressive force and displacement were obtained for sample P310 at 7612.29 N and 4.81 mm, respectively.

Among all samples, the highest failure compressive force for sample P110 was obtained as 9581.56 N, which is 332% higher than the compressive force at failure of sample P215, which is 2213.77 N. Additionally, the highest displacement for sample P110 was 5.31 mm, which is 85% higher than the displacement obtained for sample P215. Relatively, samples with pattern P1

had higher compressive force tolerance and displacement compared to samples printed with patterns P2 and P3. This is due to the uniform 50% infill density across the samples and the location of joints, which increases the load-bearing capacity. In contrast, in bending tests, samples with pattern P2 showed higher bending strength compared to samples with pattern P3, while in compression tests, samples with pattern P3 exhibited higher compressive force tolerance compared to samples with pattern P2. To better understand the failure behavior of the samples, images of some samples in **Figure 16** are visible. Additionally, given the instantaneous nature of failure, selecting a specific load for all samples for comparison was not feasible. In all cases, failure occurred after the completion of the test, manifesting as delamination between printed layers.

As evident in the images of the samples in **Figure 16**, samples with pattern P1 have the least amount of damage compared to other samples, and their failure occurs only at one of the joints without any visible failure along the edges of the structure. In

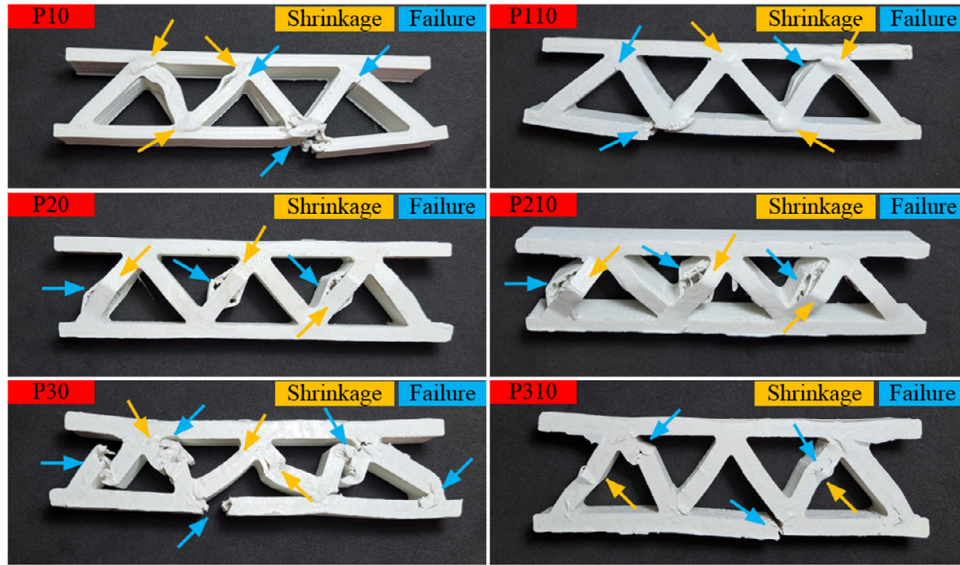


Figure 16. The images of fractured samples after compressive test.

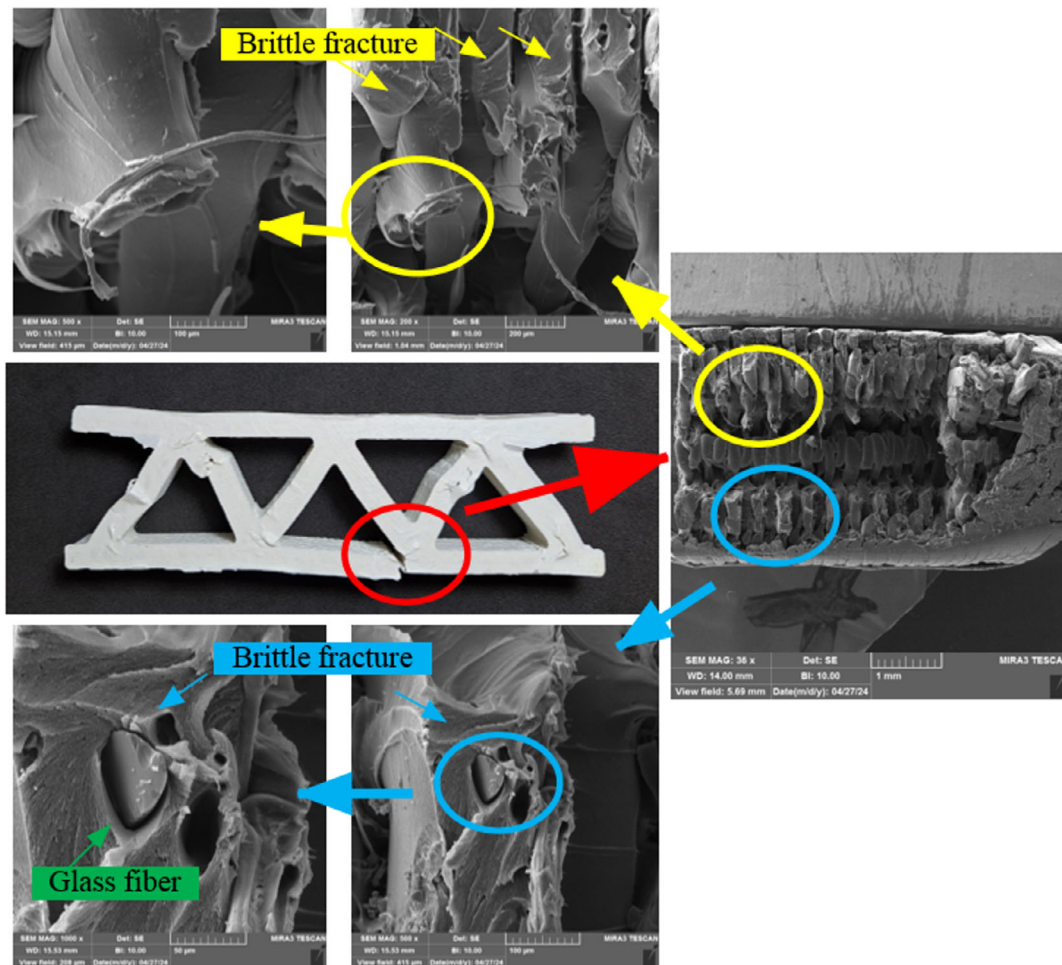


Figure 17. The SEM images of fracture cross section of P310 sample.

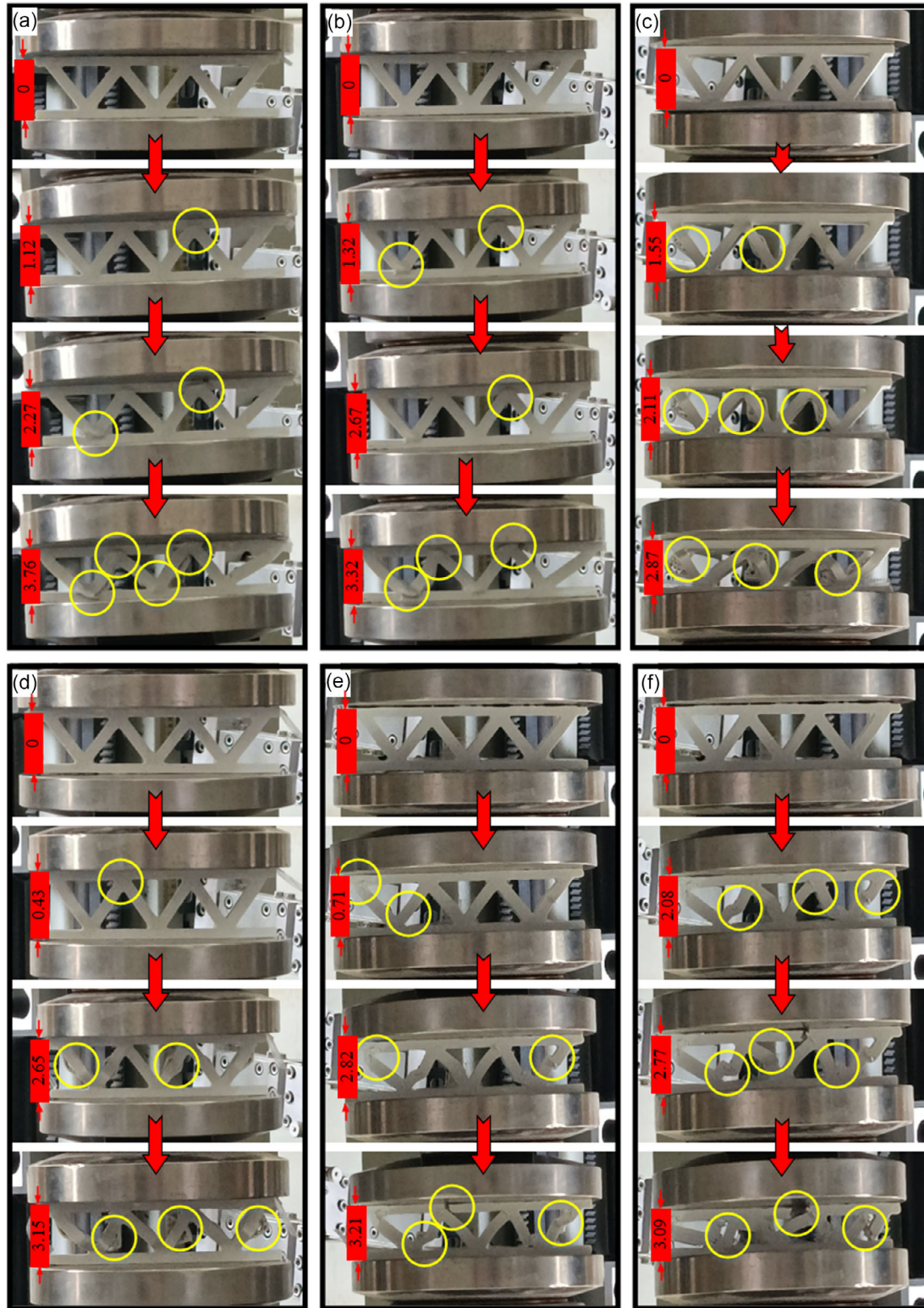


Figure 18. The process of samples' failure while compressive test a) P10, b) P115, c) P215, d) P20, e) P30, and f) P315.

contrast, in samples with pattern P2, due to having the lowest infill percentage in the central line and an increase in infill percentage with upward and downward movement of the sample, the failure locations are exactly in the middle of the edges, showing delamination between layers. In samples with pattern P3, considering their infill pattern, in addition to failure at their joints, they also experience cracking and plastic deformation in edges with lower infill percentages. In all samples, layer adhesion is observed, indicating good bonding between layers and ideal printing process parameters. For a more detailed investigation of the failure behavior, an SEM image of the fracture cross section of sample P310 is provided in **Figure 17**, where brittle fracture of printed layers and the presence of glass fibers in the base material are visible. To analyze the force application process and sample failure behavior, periodic photography was taken during compression testing, and images of the fracture process of some samples can be seen in **Figure 18**. In samples with pattern P2, fractures intensified in the middle of the sides with force application, while in other patterns, layer adhesion and failure at joints are clearly visible.

For a better understanding of the behavior of the produced samples under compressive test, a force–displacement diagram for some samples is plotted in **Figure 19**. Generally, the trend of sample behavior under applied force is similar, where displacement occurs until the moment of failure with an increase in force. The failure mode and displacement of the samples in **Figure 18** correspond to the graph obtained from the compression test in **Figure 19**. For instance, in the case of sample P10, the failure process initiated at the two connection points between the walls and the flanges on both sides of the sample, corresponding to an upper jaw displacement of ≈ 2 mm. As the compression continued and the displacement reached around 3.8 mm, the other connection points of the sample failed, followed by a decrease in the compressive force. This process occurred differently in sample P30, where the failure of all connections in the sample occurred at a displacement of ≈ 3.2 mm. However, due to the incomplete separation of the connections, the decrease in force continued gradually until around 3.8 mm.

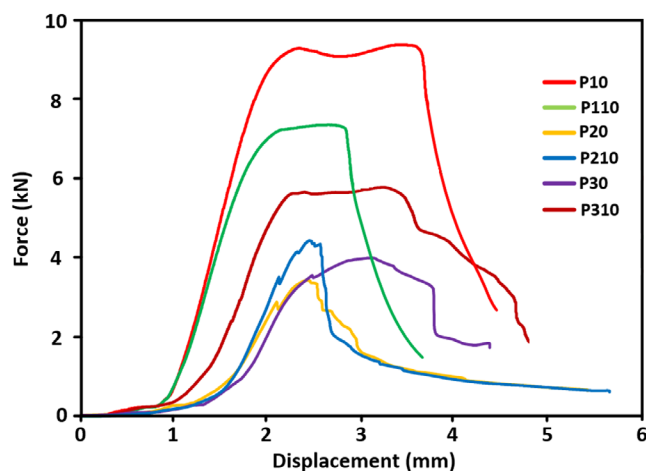


Figure 19. The force–displacement of samples after compressive test.

3.4. The Comparison between Failure Forces and Weight and Time

An important parameter used for comparing materials and components is the ratio of failure force to their weight, where a higher ratio can be considered as an advantage. The weight and breaking forces obtained for printed samples are provided in **Table 3** for comparison, and for a better comparison, the results are presented graphically in **Figure 20**. Due to the printing conditions and filaments used for producing the samples, the weight of bending and compression samples may vary slightly, and the written weight represents the average weight of two samples.

With an increase in the percentage of glass fibers in the base material and the production of samples from filaments, the weight of the samples increases due to the presence of glass fibers in them. The ratio of failure force to the weight of the produced samples increases with an increase in the percentage of glass fibers up to 10%, and then with an increase in the percentage of glass fibers up to 15%, a significant decrease is observed in this ratio. The highest ratio of failure bending force to weight for sample P110 was obtained as 73.29 N g^{-1} , which is 12% higher than sample P10, and the lowest ratio among all samples was obtained for sample P315 as 23.43 N g^{-1} , which is 212% lower than the ratio of failure bending force to weight for sample P110. Since sandwich structures can withstand higher compressive forces, the ratio of compressive force to weight for the produced samples was significantly higher. The highest ratio of failure compressive force for sample P310 was 370.51 N g^{-1} , followed by 366.05 N g^{-1} for sample P210, and in third place, a ratio of 355.80 N g^{-1} was obtained for sample P110. Relatively, the ratio of failure compressive force for samples printed with pattern P1 and then for samples with pattern P2 was obtained. The lowest ratio of compressive force to weight for sample P215 was 109.48 N g^{-1} .

Since another important parameter considered in the production of samples using additive manufacturing is the time it takes to produce the samples, another comparison was made under the

Table 3. The failure forces and weight of produced samples.

Sample	Bending failure force [N]	Compressive failure force [N]	Weight [g]	Bending failure force/weight [N g^{-1}]	Compressive failure force/weight [N g^{-1}]
P10	1669.21	4714.61	25.51	65.43	184.81
P15	1751.46	9143.61	26.62	65.79	343.49
P110	1973.62	9581.56	26.93	73.29	355.80
P115	1187.56	4085.59	27.04	43.92	151.09
P20	857.03	3133.04	17.66	48.53	177.41
P25	1008.72	4377.21	19.14	52.70	228.69
P210	1049.91	7218.55	19.72	53.24	366.05
P215	701.76	2213.77	20.22	34.71	109.48
P30	708.74	3679.10	18.46	38.39	199.30
P35	923.37	5646.21	20.99	43.99	269.00
P310	1038.66	7621.29	20.57	50.49	370.51
P315	506.49	2821.64	21.62	23.43	130.51

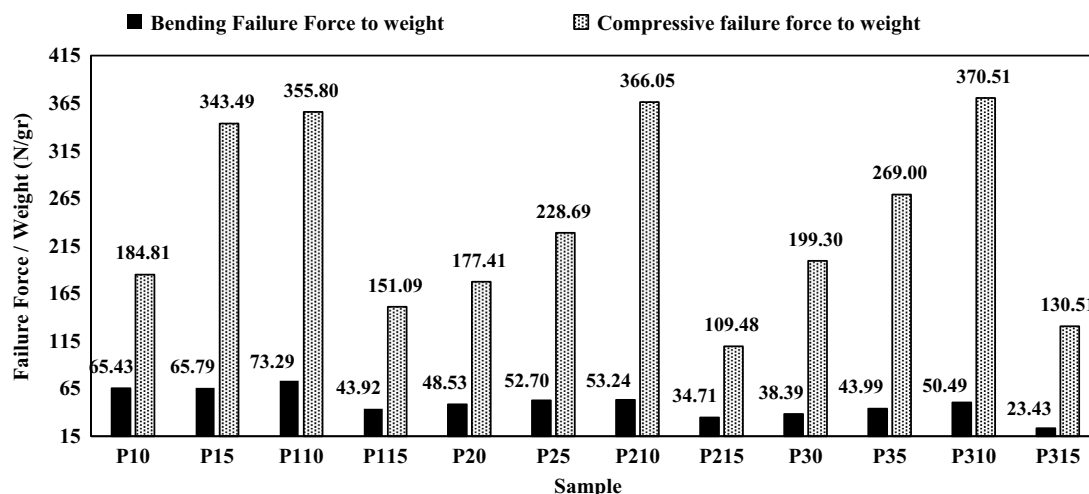


Figure 20. The graph of failure force to weight of produced samples.

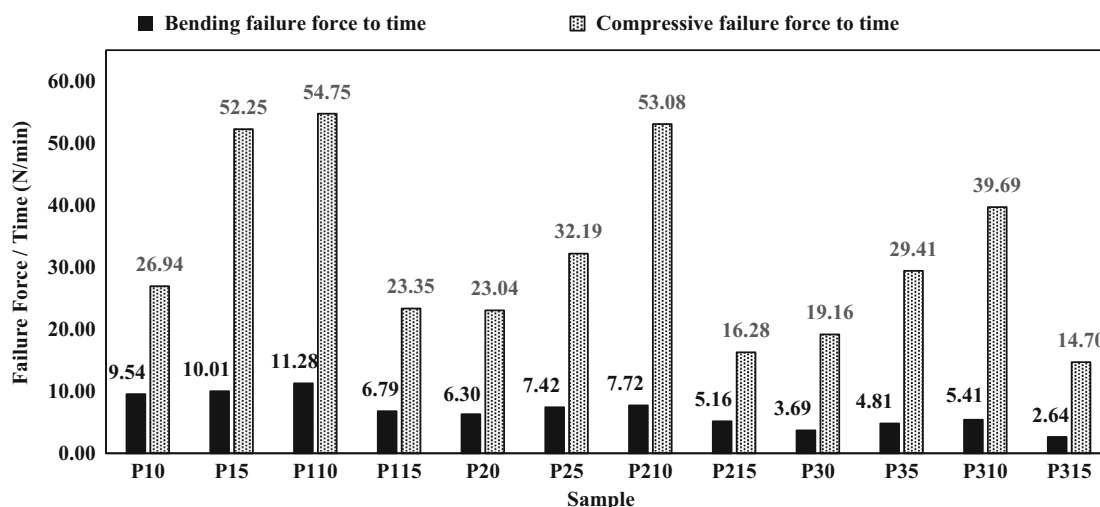


Figure 21. The graph of failure force to produced time of samples.

title of the ratio of failure force to production time. The production and printing time for samples with pattern P1 was 175 min, and this time for producing samples with patterns P2 and P3 was 136 and 192 min, respectively. It is worth mentioning that there was not much difference in production time between samples with a specific pattern and different filaments. By dividing the bending and compressive failure forces of the samples by the production time of the samples, a force-to-weight ratio diagram is shown in **Figure 21**. The overall trend of the force-to-time ratio is consistent with other results, where with an increase in the percentage of glass fibers up to 10%, this ratio increases, and with an increase in the percentage of glass fibers up to 15%, a decreasing trend of force to weight occurs. The highest ratio of failure bending force to time for sample P110 was 11.28 N min^{-1} , which is 66% higher than sample P115. For samples produced with pattern P2, the highest ratio of failure bending force to time was 7.72 N min^{-1} for sample P210, and the lowest was 5.16 N min^{-1} for sample P215. The lowest force-to-time

ratio for sample P315 was 2.64 N min^{-1} , which is 104% and 82% lower than samples P310 and P35. The highest ratio of failure compressive force to time was also obtained for sample P110 as 54.75 N min^{-1} , which is 272% higher than the ratio of failure compressive force to time for sample P315. The highest failure compressive force-to-time ratios for samples printed with patterns P2 and P3 was 53.08 N min^{-1} for sample P210 and 39.69 N min^{-1} for sample P310.

4. Conclusion

In this study, corrugated core sandwich panels were produced using additive manufacturing with ABS filaments reinforced with varying percentages of glass fibers (0, 5, 10, and 15%). Three different infill density patterns were employed: a uniform 50% density, a gradient from 15% to 60%, and a variable density from 25% to 75% at critical points. These results demonstrate

the significant impact of glass fiber reinforcement and infill density patterns on the mechanical properties of 3D-printed corrugated core sandwich panels. Optimizing these parameters can lead to the development of high-strength, light-weight structures suitable for various industrial applications. The panels were subjected to bending and compressive tests, yielding the following results. 1) The highest failure bending force for sample P110 was 1973.62 N, which is 289% higher than that of sample P315 (506.49 N). The highest displacement rate during the bending test for sample P110 was 4.05%, while the lowest displacement was 2.52% for sample P315. An increase in glass fiber percentage up to 10% enhanced the displacement rate, but further increases to 15% led to premature failure and decreased displacement. 2) The highest failure compressive force for sample P110 was 9581.56 N, 332% higher than that of sample P215 (2213.77 N). The highest displacement for sample P110 was 5.31 mm, 85% higher than the displacement for sample P215. 3) The ratio of failure bending force to weight for sample P110 was 73.29 N g^{-1} , 12% higher than for sample P10. The lowest ratio was for sample P315 at 23.43 N g^{-1} , 212% lower than for sample P110. The highest ratio of failure compressive force to weight was for sample P310 at 370.51 N g^{-1} , followed by 366.05 N g^{-1} for sample P210 and 355.80 N g^{-1} for sample P110. 4) The highest ratio of failure bending force to time for sample P110 was 11.28 N min^{-1} , 66% higher than for sample P115. The lowest ratio was for sample P315 at 2.64 N min^{-1} , 104% and 82% lower than for samples P310 and P35, respectively. The highest ratio of failure compressive force to time was also for sample P110 at 54.75 N min^{-1} , 272% higher than for sample P315.

Based on the results obtained, the varying infill density pattern for sandwich panels has a negligible impact on their strength, and a uniform distribution of infill density yields the best results. To further enhance the compressive strength of the panels, other reinforcing fibers such as carbon, as well as glass fibers with different dimensions or arrangements, can be utilized. Investigating the effects of varying cell geometry and interface wall geometry in the panels could be carried out in the future research.

Acknowledgements

M.B. acknowledges the support by the RAEng/Leverhulme Trust Research Fellowship (grant no. LTRF-2324-20-129).

Conflict of Interest

The authors declare no conflict of interest.

Author Contributions

Ali Sadooghi: Conceptualization (lead); Data curation (lead); Formal analysis (lead); Investigation (lead); Methodology (lead); Supervision (equal); Validation (lead); Visualization (lead); Writing—original draft (lead). **Mohammad Reza Ebrahimian:** Conceptualization (equal); Data curation (equal); Formal analysis (equal); Investigation (equal); Methodology (equal); Supervision (equal); Writing—review & editing (equal). **Seyed Jalal Hashemi:** Formal analysis (lead); Investigation (equal); Methodology (equal); Software (equal); Writing—review & editing (equal). **Rasool**

Sayar: Data curation (equal); Investigation (equal); Software (supporting); Validation (supporting); Writing—review & editing (supporting). **Kaveh Rahmani:** Formal analysis (equal); Investigation (equal); Methodology (equal); Software (lead); Validation (lead); Visualization (equal); Writing—review & editing (equal). **Mahdi Bodaghi:** Conceptualization (lead); Formal analysis (lead); Investigation (equal); Methodology (equal); Project administration (equal); Supervision (equal); Validation (supporting); Writing—review & editing (equal).

Data Availability Statement

The data that support the findings of this study are available from the corresponding author upon reasonable request.

Keywords

additive manufacturings, composites, corrugated cores, glass fibers, sandwich panels

Received: August 4, 2024

Revised: October 31, 2024

Published online: November 27, 2024

- [1] S. M. Zaharia, L. A. Enescu, M. A. Pop, *Polymers* **2020**, *12*, 1740.
- [2] G. Hu, M. Bodaghi, *Adv. Eng. Mater.* **2023**, *25*, 2300334.
- [3] O. Fourmann, M. K. Hausmann, A. Neels, M. Schubert, G. Nyström, T. Zimmermann, G. Siqueira, *Carbohydr. Polym.* **2021**, *259*, 117716.
- [4] J. Sedláč, Z. Joska, L. Hrbáčková, E. Juříčková, D. Hrušecká, O. Horák, *Manuf. Technol.* **2022**, *22*, 733.
- [5] P. Wu, J. Wang, X. Wang, *Autom. Constr.* **2016**, *68*, 21.
- [6] G. Ye, H. Bi, Y. Hu, *Compos. Struct.* **2020**, *233*, 111706.
- [7] P. V. Yap, M. Y. Chan, S. C. Koay, *J. Phys. Sci.* **2021**, *32*, 87.
- [8] B. Coppola, N. Cappetti, L. Di Maio, P. Scarfato, L. Incarnato, *Materials* **2018**, *11*, 1947.
- [9] R. T. L. Ferreira, I. C. Amatte, T. A. Dutra, D. Bürger, *Composites, Part B* **2017**, *124*, 88.
- [10] D. Wannarong, T. Singhanart, *Eng. J.* **2022**, *26*, 27.
- [11] A. Yousefi, S. Jolai, M. L. Dezaki, A. Zolfagharian, A. Serjouei, M. Bodaghi, *Adv. Eng. Mater.* **2023**, *25*, 2201189.
- [12] R. Hamzehei, M. Bodaghi, J. A. Iglesias Martinez, Q. Ji, G. Ulliac, M. Kadic, C. Wang, A. Zolfagharian, N. Wu, *Adv. Eng. Mater.* **2023**, *25*, 2201842.
- [13] D. Rahmatabadi, M. Aberoumand, K. Soltanmohammadi, E. Soleyman, I. Ghasemi, M. Baniassadi, K. Abrinia, M. Bodaghi, M. Baghani, *Adv. Eng. Mater.* **2023**, *25*, 2201309.
- [14] P. Yadav, A. Sahai, R. S. Sharma, *J. Inst. Eng. (India): Ser. C* **2021**, *102*, 197.
- [15] P. K. Mishra, P. Senthil, S. Adarsh, M. S. Anoop, *Compos. Commun.* **2021**, *24*, 100605.
- [16] A. P. Agrawal, V. Kumar, J. Kumar, P. Paramasivam, S. Dhanasekaran, L. Prasad, *Heliyon* **2023**, *9*, e16531.
- [17] M. Q. Tanveer, A. Haleem, M. Suhaib, *SN Appl. Sci.* **2019**, *1*, 1701.
- [18] I. Wegner, M. Campbell, in *2024 Regional Student Conf.*, American Institute of Aeronautics and Astronautics **2024**, p. 81359.
- [19] L. Cheng, X. Liang, E. Belski, X. Wang, J. M. Sietins, S. Ludwick, A. To, *J. Manuf. Sci. Eng.* **2018**, *140*, 105002.
- [20] A. Kalani, J. Vadher, S. Sharma, R. Jani, *El-Cezeri* **2022**, *9*, 1121.
- [21] V. Zal, A. Sadooghi, S. J. Hashemi, K. Rahmani, A. H. Roohi, H. Khodayari, J. Babazadeh, *Arabian J. Sci. Eng.* **2024**, *49*, 11167.
- [22] M. Bodaghi, A. Sadooghi, M. Bakhshi, S. J. Hashemi, K. Rahmani, M. Keshavarz Motamedi, *Adv. Mater. Interfaces* **2023**, *10*, 2300337.